Evidence of Oxidation of Aromatic Hydrocarbons by Chloromethyl Radicals: Reinvestigation of Intersolute Hole Transfer Using Pulse Radiolysis

Kiminori Ushida,*,† Yoichi Yoshida,‡ Takahiro Kozawa,‡ Seiichi Tagawa,‡ and Akira Kira†

The Institute of Physical and Chemical Research (RIKEN), 2-1 Hirosawa, Wako, Saitama, 351-0198 Japan, and The Institute of Industrial Research, Osaka University, 8-1 Mihogaoka, Ibaraki, Osaka, 567-0047 Japan

Received: October 26, 1998; In Final Form: March 30, 1999

Intersolute hole transfer ($A^{\bullet+} + B \rightarrow A + B^{\bullet+}$) was reinvestigated using nanosecond pulse radiolysis in fluid solutions of dichloromethane (A, biphenyl; B, naphthacene, rubrene). Under our new experimental conditions where the concentration of the second solute [B] was kept higher than 0.5 mM, the kinetics of the hole transfer was observed within 500 ns after irradiation, at which time the geminate recombination process with counterpart anionic species was also observed. On the basis of the analysis with the Smoluchowski equation, the second-order rate constants of hole transfers were successfully obtained. Moreover, we confirmed the existence of another slow oxidation of the second solute B by the solvent neutral radical $CH_2Cl^{\bullet}$ formed from the electrons ejected during the initial ionizing process. This reaction is a kind of electron transfer with a charge separation that has never been confirmed, but should generally exist in an irradiated solution of halogenated compounds. In our present case, more than 30% of $B^{\bullet+}$'s were formed through this side reaction. We clarify the formation of two ion pairs on one ionizing event, which will have a great impact on the understanding of the results of product analyses in radiation chemistry. Examination using ab initio molecular orbital calculation of two dissociative electron transfers is also presented.

Introduction

The contribution of achievements in radiation chemistry to our understanding of electron transfer (ET) reactions started in the early days of pulse radiolysis.[1] Dorfman and co-workers[2,3] provided a number of examples of intersolute electron and hole transfer between aromatic hydrocarbons dissolved in alcohol,[2] ethers,[2] and halogenated compounds.[3]

Their method was adopted in low-temperature matrix studies[4,5] where the influence of diffusion could be excluded. Finally, using a series of linked molecular systems, Closs, Miller, and their co-workers[6] succeeded in reproducing the inverted region that had been predicted by Marcus[4,7] and in providing much information about the distance dependence of the matrix element of electron transfer.[8] Pulse radiolysis is one of the most valuable techniques of realizing a real-time observation of ET with a charge shift between two solute molecules and can be easily applied to various organic systems, whose basic molecular parameters (dielectric constants,[9] ionization potentials,[10] electron affinity,[11] oxidation and reduction potentials[12]) are available. A number of researchers now are engaged in this kind of study to discuss the validity of the Marcus theory.[13]

The idea of using two solutes in pulse radiolysis, which was originally proposed by Dorfman's group,[2,3] has a number of advantages in the determination of electron transfer rate constants. For a positive charge shift, the total process is generally expressed by,

$$S \rightarrow S^{\bullet+} + e^- \quad (1)$$

$$S^{\bullet+} + A \rightarrow S + A^{\bullet+} \quad (2)$$

$$S^{\bullet+} + B \rightarrow S + B^{\bullet+} \quad (3)$$

$$A^{\bullet+} + B \rightarrow A + B^{\bullet+} \quad (4)$$

where S, A, and B are the solvent and the two solutes, respectively. The case of negative charge shift can be described in a similar manner. Most of the previous experiments were performed with [A]/[B] > 1000 and by observing only reaction 4 with slow measurement (>1 mS). Although slow observation is free of the influence of geminate ion recombination,[14] which also contributes to the decrease of the amounts of $A^{\bullet+}$ and $B^{\bullet+}$, the influence of slow side reactions has not been clarified.

Recent progress in the understanding of the geminate ion recombination process of irradiated fluid solution enabled us to reproduce the survival curve of geminate ion pairs produced by the initial ionization.[15,16] The assumption that a large fraction of ion pairs are isolated from each other can be applied to discuss the nanosecond kinetics in the experiment with low linear energy transfer (LET) irradiation sources, such as electron beams.[1] The initial distribution function of the separation of the geminate ion pair is assumed and the Smoluchowski equation[17] is then applied to reproduce the nonexponential time profiles and the free ion yield.[15,16]

Nowadays, there is no reason to ignore the observation of fast electron transfer, which competes with the geminate ion recombination. If we can apply a high concentration of solutes, the observation of ET should be more reliable, excluding any side reactions induced by unidentified byproducts existing in small concentration in the irradiated solution.

In this article, we report the reexamination of the hole transfer process with charge shifting in irradiated fluid solution of dichloromethane (DCM). This kind of system had rarely been treated after the series of works by Dorfman and co-workers. In our present study, biphenyl radical cations[18,19] were used as the hole donor ($A^{\bullet+}$), and naphthacene and rubrene were the hole acceptors (B). Since the concentration of B, [B], was in the range 0.8−3.2 mM, the diffusion-controlled hole transfer process ($k_{HT} = 1.1 \times 10^{10}$, 0.65×10^{10} [M^{-1} s^{-1}] for naphthacene and rubrene, respectively) was observed in the same time range as the geminate ion recombination.[15,16]

* To whom correspondence should be addressed. E-mail: kushida@postman.riken.go.jp. Fax +81-48-462-4668.

† The Institute of Physical and Chemical Research.

‡ The Institute of Industrial Research.

10.1021/jp9841900 CCC: $18.00
Published on Web 05/29/1999

In the present study, we observed slow oxidation of aromatic hydrocarbons by a chloromethyl radical. This radical is well-known as an electrophile in organic chemistry, but the direct observation of the oxidation process is rarely reported, probably because the transient observation of this radical is very difficult. Although our present study is an indirect observation, it is new evidence of the electron transfer of the charge-separating type caused by this radical.

Experimental and Computational Section

Spectral grade dichloromethane (DCM) from Merck was used without further purification. Zone-refined biphenyl (BP) from Tokyo Chemical Industry Co. Ltd. (TCI) was purified by recrystallization from ethanol solution. Naphthacene of GR grade (NP) from TCI was purified by sublimation in a vacuum, and rubrene of SP grade (RB) from TCI was purified by recrystallization from benzene solution in the dark. Molecular parameters in the literature are summarized in Table 1S. The solutions were bubbled with Ar for 5−10 min before each measurement in a quartz cell with a 2 cm path length.

Nanosecond pulse radiolysis was performed at the 35 MeV Linac of the University of Tokyo at Tokai, Ibaraki, Japan. Transient absorption spectra at 600−1000 nm were measured using a Si photodiode (S-1722-01) from Hamamatsu Photonics through a monochromator (Ohyo-Koken MC-10N) using a Xe flash lamp (EG&G FX279U) as a probing light source. Other details of measurement have been described elsewhere.[20]

All the data were recorded on a digital oscilloscope (Tektronix: SDC1000) as time profiles with 1024 data points at each wavelength in the range 600−950 nm with an equal separation of 10 nm. Spectral fitting and simulation were performed on several kinds of DOS/V personal computers using original programs. Spectral fitting and simulation were performed using the equations discussed in the Appendix.

Ab initio molecular orbital calculation was performed on a GAMESS program incorporated on a DEC 3000/900 or a DEC 3000/700 workstation at RIKEN. The program was kindly provided by Gordon et al. through the Internet.[21]

Results and Discussion

Measurement of Solution with a Single Solute and Determination of Spectra for Each Radical Cation. First we performed measurements of transient absorption in the range of 600−1000 nm for DCM solutions of BP, NP, and RB to determine the spectral line shapes for their radical cations. Almost saturated solutions of each compound were used: 100, 10, and 1.6, for BP, NP, and RB, respectively. Depending on the solute concentration, weak, broad absorption bands, probably due to solvent holes, are observed at 600−700 nm range within 100 ns after irradiation.[22] Moreover, a slight sharpening of spectral peaks of radical cations was also observed within the initial 100 ns. To exclude the contribution of holes and to determine the spectral line shapes for the relaxed radical cation, we took the averaged value of 100−150 ns for each wavelength to obtain the spectral line shapes shown in Figures 1a−c. Each spectrum was obtained as a splined curve of averaged data and normalized.

Dashed lines in Figure 1 indicate spectral line shapes reproduced from the results of Shida's matrix study.[23] Our data and the reference data are normalized to the same magnitudes of the integrated oscillator strength on an energy-linear scale. The extremely sharp profiles obtained in the matrix study seem to be due to a kind of Shpol'skii matrix effect.[24] Small spectral peak shifts <20−30 nm should be attributed to matrix and solvent effects.

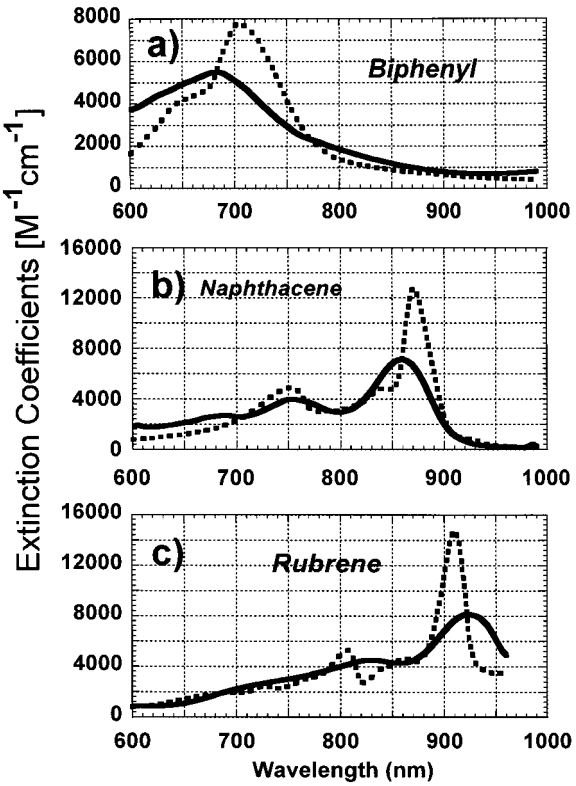

Figure 1. Spectra of radical cations of (a) biphenyl, (b) naphthacene, and (c) rubrene formed in dichloromethane determined from the results of nanosecond pulse radiolysis (solid lines). The vertical scales in (b) and (c) are adjusted to the new extinction coefficient obtained from our present results (see text). Dashed lines are spectra of the same radical cation observed in γ-irradiated low-temperature matrix reproduced from ref 23, of which the integrated oscillator strength is normalized to the results of our present pulse radiolysis.

The vertical scale for the spectrum of BP radical cations was taken to be a reported value of $\epsilon = 3.7 \times 10^3$ M^{-1} cm^{-1} at 600 nm.[18] Although the extinction coefficient of $BP^{\bullet+}$ in refs 18a and 18c was obtained in hydrocarbons, we use this value in the present experiment with dichloromethane as the solvent. It can be justified because the spectral peak position and the total line shape of this band are similar in both solvents. The two other vertical scales ($NP^{\bullet+}$, $RB^{\bullet+}$) were determined from our present analysis as values relative to $BP^{\bullet+}$ (see following section). In the matrix study, extinction coefficients were not obtained because the low solubility in the matrix prohibits complete charge scavenging.[25] Therefore, the vertical scale for the matrix data in Figure 1 have no meanings other than the values obtained by the normalization for comparison with our present data.

Analysis of Decay Kinetics of the Biphenyl Radical Cation Based on Smoluchowski Equation. The decay profiles of the transient absorption of $BP^{\bullet+}$ at 690 nm are indicated in Figure 2 for (a) 100 mM and (b) 10 mM solutions of BP in DCM. They can be analyzed, using the Smoluchowski equation,[17] as a geminate ion recombination process. The results of simulation are also indicated in the same figure but overlap in the most part of the decay curves. A complete set of analytical formulations suitable for these kinds of problems has already been presented by Tachiya[26] and has been successfully applied to a number of irradiated liquid solutions.[16]

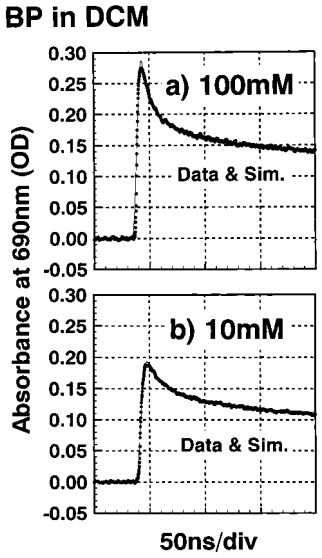

Figure 2. Decay profiles of the transient absorption at 690 nm observed for (a) 100 mM and (b) 10 mM solutions of biphenyl in dichloromethane. Fitted lines obtained by the simulation in the present work are also indicated with solid lines although the majority of the curves overlaps with the experimental results. Adjusted parameters are summarized in Table 1.

If the concentration of the solute is sufficiently low, most of the ionization processes take place in the solvents immediately after irradiation as

$$CH_2Cl_2 \rightarrow CH_2Cl_2^{\bullet+} + e^- \quad (5)$$

to form a geminate ion pair. Ejected electrons are captured by another solvent molecule and produce chloride anions and neutral radicals through dissociative electron attachment (DEA)[27] as

$$CH_2Cl_2 + e^- \rightarrow CH_2Cl^{\bullet} + Cl^- \quad (6)$$

Normally, process 6 is very fast because of the high concentration of solvent molecules. The positive charge is scavenged by BP with a second-order rate constant k_{QA} as large as that of the diffusion-controlled reaction driven by a large difference in the ionization potentials (CH_2Cl_2, 10.8 eV; BP, 8.2 eV). That is,

$$CH_2Cl_2^{\bullet+} + BP \rightarrow CH_2Cl_2 + BP^{\bullet+} \quad (7)$$

Under the present experimental conditions ([BP] > 10 mM), reactions 6 and 7 complete within a few nanoseconds.

As reported by Alfassi et al.,[28] there should be a small contribution of the excited state of the solvent releasing a chlorine atom as

$$CH_2Cl_2^* \rightarrow CH_2Cl^{\bullet} + Cl^{\bullet} \quad (8)$$

If the scavenging process (7) is not completed, the excited state of the solvent can be produced on geminate recombination as

$$CH_2Cl_2^{\bullet+} + e^- \rightarrow (CH_2Cl_2^*) \rightarrow CH_2Cl^{\bullet} + Cl^{\bullet} \quad (8')$$

The fraction (G value) of (8) is believed to be far smaller than that of (5) and (6), and (8′) should be also unimportant under our experimental condition ([BP] > 10 mM). Probable generation of chlorine atom by (8) and (8′) will be discussed in a following section in relation to the side reaction found in our experiment.

Since the electron beam used in the present pulse radiolysis is a typical low LET irradiation source, we can assume that the geminate ion pair formed by (5) is isolated from other ion pairs. This assumption can be applied satisfactorily to analyze the kinetics 1−100 ns. The effect of multiple ionization in one spur may be revealed in early events (within 1ns after irradiation) and may affect the quantitative discussion of product yields.

The initial separation of the geminate ion pair formed immediately after irradiation depends on the excess kinetic energy shared on both particles. For the ionization process produced by the radiation chemical method, we have to assume the initial distribution function of the initial separation. Despite this limitation, however, this procedure has been successfully applied to reproduce the kinetics of the geminate recombination in a number of liquid systems.[15,16]

Under the present condition where a large amount of DCM molecules exist as the solvent, the DEA (6) undergoes extremely rapid reaction and almost no noncaptured electrons remain after 10 ps. Thus, since the sole effective negative charged species is Cl^-, the only two geminate recombination processes to be considered are

$$CH_2Cl_2^{\bullet+} + Cl^- \rightarrow (\text{products: probably } CH_2Cl^{\bullet} + HCl) \quad (9)$$

$$BP^{\bullet+} + Cl^- \rightarrow (\text{products}) \quad (10)$$

in both of which the attractive potential of Coulombic force considerably accelerates.[15−17] Since both of reactions 8 and 9 are inhomogeneous, they should be analyzed using the Smoluchowski equation as

$$\frac{\partial w}{\partial t} = D\nabla\left(\nabla w + w\frac{1}{kT}\nabla V\right) \quad (11)$$

where w, D, k, and V are the probability density function of geminate ions, the sum of the diffusion coefficients of ions, the Boltzmann constant, and the Coulomb potential, respectively. The initial separation of ion pair r_0 should be applied to (11) as a boundary condition. Hong and Noolandi have derived the analytical solution of (11) for a single value of the initial separation r_0 of the geminate ion pair.[29] For the present numerical simulation, we use the survival probability of ion pair $W^0(r_0,t)$. In a manner identical to that in the previous study,[16] we assumed the initial distributions of the geminate ion pairs to be

$$\rho(r_1,r_0) = (1/r_0)\exp(-r_1/r_0) \quad \text{(an exponential function)} \quad (12)$$

where new r_0 is the mean value of the initial separation of the ion pair. Another possible choice of the initial distribution function is

$$\rho(r_1,r_0) = (4{r_1}^2/\pi^{1/2}{r_0}^3)\exp(-{r_1}^2/{r_0}^2) \quad \text{(a Gaussian function)} \quad (13)$$

The distribution functions in (12) and (13) are already normalized as

$$\int_0^\infty \rho(r_1, r_0)\, dr_1 = 1 \quad (14)$$

With these formulations, the survival probability of the ion pair $W_i^0(t)$ (i = 1, 2, ...) is given by

$$W_i^0(t) = \int_0^\infty \rho(r_1, r_0)\, W_i^0(r_1, t)\, dr_1 \quad (15)$$

The positive charge is scavenged by BP on reaction 7 to form another geminate pair, resulting in the delayed geminate recombination (10).

In our present experiment, the diffusion constant used in (11) can be substituted by that of Cl^- because only the mobility of Cl^- should be extremely large.[18] We additionally assumed that the distance distribution would not be disturbed by the scavenging process (7). In such a situation, simplification can be achieved by assuming that the recombination processes of the two kinds of geminate pairs in (9) and (10) are identical. In other words, the geminate recombination kinetics are unchanged after the scavenging process (7). Therefore, a simple set of equations is obtained:

$$[CH_2Cl_2^{\bullet+}] = W_1(t) = W_1^0(t)\exp(-k_{QA}c_A t) \quad (16)$$

$$[BP^{\bullet+}] = W_2(t) = W_1^0(t)\{1 - \exp(k_{QA}c_A t)\} \quad (17)$$

where $c_A = [BP]$.

We could successfully simulate the experimental decay curve in Figure 2 for two concentrations using the same parameters and under the assumption of the exponential distribution function of (12). The Gaussian function (13) did not reproduce the experimental results especially in the early period (<50 ns). In the fitting of geminate recombination curves, the adjustment for the line shape in the early period (<20 ns) should be important and the figures (Figures 2, 4, and 6 and Figure 1S) indicate the 0−200 ns area to stress this agreement. The decay curve of $BP^{\bullet+}$ without the second solute had a long tail and did not fall off after several microseconds due to the formation of free ion radicals. The value of the applied diffusion constant was 1×10^{-5} cm^2 s^{-1}, which is smaller than that previously used by Washio et al.[30] for CCl_4 solution (9×10^{-5} cm^2 s^{-1}). This should be the effect of the large dielectric constant (ϵ_r = 8.93 at 25 °C) of DCM,[9] which captures Cl^- effectively.

The approximate value of Onsager length (r_c = 65 Å) was directly obtained from the dielectric constant.[9] Other optimized parameters are $k_{QA} = 5 \times 10^{10}$ M^{-1} s^{-1} (second-order quenching rate constant of (7)), r_0 = 33 Å (mean value of the initial separation), and $D = 1 \times 10^{-5}$ cm^2 s^{-1} (diffusion constant of Cl^- in DCM). These parameters are used in all the simulations in the present paper. The magnitude of the quenching rate ($k_{QA} = 5 \times 10^{10}$ M^{-1} s^{-1}) is somewhat large, probably because there may be a contribution from the high mobility of the solvent hole. Other quenching rates (k_{QB} for NP, RB) obtained in the present work also exhibit the same tendency.

Analysis of Intersolute Hole Transfer from $BP^{\bullet+}$ to NP. The three-dimensional (3D) result of pulse radiolysis for the mixed solution of BP (10 mM) and NP (1.6 mM) in DCM is shown in Figure 3a. It is clear that the initial line shape of the absorption spectrum is mainly due to $BP^{\bullet+}$ and changes to that of $NP^{\bullet+}$ at 200 ns after irradiation. This indicates that the intersolute hole transfer,

$$BP^{\bullet+} + NP \rightarrow BP + NP^{\bullet+} \quad (18)$$

seems to take place. We defined k_1 as the second-order rate constant for (18) on the assumption that this process is a homogeneous one.

Under the assumption that these 3D data can be approximately reproduced by summing the spectra of $BP^{\bullet+}$ and $NP^{\bullet+}$, we automatically extracted the most probable time profiles for two components by the method described in the Appendix. The reproduced 3D result is also shown in Figure 3b, and indicates small contributions from other species; fluctuation of experimental condition can be neglected. From the comparison between two 3D figures, we can find that the nonexponential time profiles are completely reproduced in the simulation at any time and any wavelength. Therefore, it should be concluded that the analysis using only two components is sufficiently reasonable and that only a small contribution of other species exists in this area of wavelength (600−950 nm).

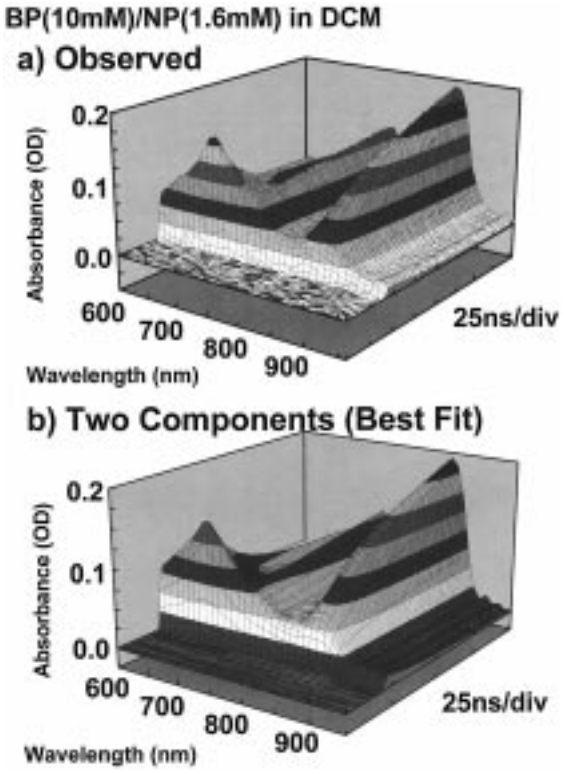

Figure 3. Three-dimensional transient absorption spectrum obtained by pulse radiolysis of the [biphenyl] = 10 mM and [naphthacene] = 1.6 mM mixed solution in dichloromethane (a) and its simulation (b). Simulation parameters are summarized in Table 1.

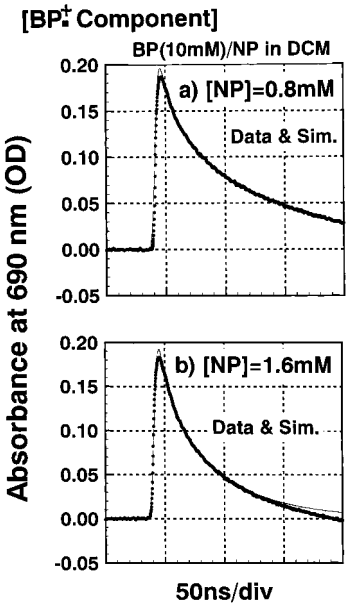

Figure 4. Kinetics of biphenyl radical cation ($[BP^{\bullet+}]$) extracted from the results of pulse radiolysis of DCM/BP/NP solution. [BP] = 10 mM (constant) and [NP] = (a) 0.8 and (b)1.6 mM. Simulation curves which were obtained from (21) with parameters summarized in Table 1 are indicated in each figure with solid lines.

Extracted decays of $BP^{\bullet+}$ for [NP] = (a) 0.8 mM and (b) 1.6 mM are indicated in Figure 4. The decay curve without NP ([NP] = 0 mM) has been already shown in Figure 2b.

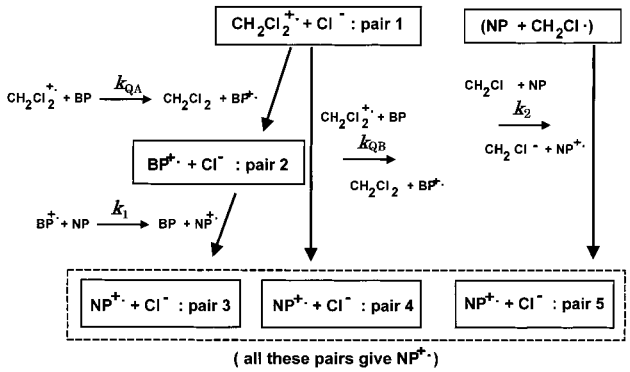

Figure 5. Schematic of total electron transfer process for DCM/BP/NP systems. Five kinds of geminate ion pairs (pair 1−5) can be considered, as shown in the scheme. In the present analysis, it is assumed that the geminate recombination process is unchanged for all ion pairs in the scheme.

When NP is added as the second solute, the second hole scavenging process takes place as

$$CH_2Cl_2^{\bullet+} + NP \rightarrow CH_2Cl_2 + NP^{\bullet+} \qquad (19)$$

with the rate constant k_{QB}. The total process is summarized in the scheme shown in Figure 5. Three kinds of ion pairs (pair 3−5) are newly considered. Pair 3 is produced from the hole transfer (18) and pair 4 from the direct charge scavenging (19). (For pair 5, explanation will be given later.) For pairs 3−5, the same assumption that the recombination process is unchanged after (18) or (19) is made. The mobilities of positive species ($CH_2Cl_2^{\bullet+}$, $BP^{\bullet+}$, $NP^{\bullet+}$) are different, and therefore the rate constants of geminate recombination processes should be different. Among these, however, the recombination with $CH_2Cl_2^{\bullet+}$ (eq 9) can be neglected after 10 ps because the yield of positive charge scavenge is high due to the sufficiently high concentration of solutes (>10 mM in total). Other geminate recombination processes involving two aromatic radical cations are determined by the mobility of Cl^-, which is very large, and the difference in the mobility of cationic species can be neglected.

Because of the existence of NP in higher concentration than the ionized species, (16) and (17) must be modified to

$$[CH_2Cl_2^{\bullet+}] = W_1(t) = W_1^0(t)\exp\{-(k_{QA}c_A + k_{QB}c_B)t\} \qquad (20)$$

$$[BP^{\bullet+}] = W_2(t) = W_1^0(t)\frac{k_{QA}c_A}{k_{QA}c_A + k_{QB}c_B}[\exp\{k_1c_Bt\} - \exp\{-(k_{QA}c_A + k_{QB}c_B)t\}] \qquad (21)$$

and the survival curve of pairs 3 and 4 can be written as[31]

$$W_3(t) = W_1^0(t)\frac{k_{QA}c_Ak_1c_B}{k_{QA}c_A + k_{QB}c_B - k_1c_B} \times \left[\frac{1 - \exp\{-k_1c_Bt\}}{k_1c_B} - \frac{1 - \exp\{(k_{QA}c_A + k_{QB}c_B)t\}}{k_{QA}c_A + k_{QB}c_B}\right] \qquad (22)$$

$$W_4(t) = W_1^0(t)\frac{k_{QB}c_B}{k_{QA}c_A + k_{QB}c_B}[1 - \exp\{(k_{QA}c_A + k_{QB}c_B)t\}] \qquad (23)$$

where $c_A = [BP]$ and $c_B = [NP]$. The simulation curves obtained from (21) are also shown in Figure 4 and k_1 was determined as 1.1×10^{10} [M^{-1} s^{-1}].

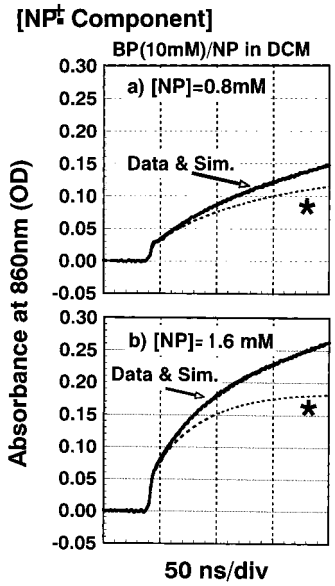

Figure 6. Kinetics of the naphthacene radical cation ([$NP^{\bullet+}$]) extracted from the results of pulse radiolysis of DCM/BP/NP solution. [BP] = 10 mM (constant) and [NP] = (a) 0.8 and (b) 1.6 mM. Simulation curves obtained from (22), (23), and (25) with parameters summarized in Table 1 are also indicated in the figures, although the majority of the curves overlaps with the experimental results. The profile component from hole transfer from $BP^{\bullet+}$ (18) is indicated by the dashed line (marked with asterisks*). Almost 30% of [$NP^{\bullet+}$] is formed through the extra process (24), as indicated in the figure.

The formation curve of $NP^{\bullet+}$ was also obtained as shown in Figure 6. However, simulation using (22) and (23) cannot reproduce the experimental curve shown by asterisks. Since the spectral line shape of the rising component ($NP^{\bullet+}$) seems unchanged throughout the process, as seen in the 3D figure of Figure 3, the possibility of the formation of dimer ion radicals can be excluded. We must include another oxidation process that can be expressed as a pseudo-first-order reaction to [NP] with a second-order rate constant k_2.

$$(\text{unknown}) + NP \rightarrow (\text{unknown}') + NP^{\bullet+} \qquad (24)$$

Since (24) is an oxidation process, the possibility of unimolecular reaction can be excluded. This component is treated as pair 5 in Figure 4. The concentration of the unknown product should be far smaller than the initial concentration of NP. Although the degradation of pair 5 is unknown, we presumed that (24) proceeds independently of the geminate processes (8) and (9) and obtained

$$W_5(t) = \alpha\{1 - \exp(-k_2c_Bt)\} \qquad (25)$$

where α is the relative yield of this reaction normalized for one ionizing event. In the pseudo-first-order reaction, the yield of (24) is determined by the concentration of the unknown counterpart. If the unknown species exist in the same concentration as that of the ionizing event, α becomes unity.

We could successfully reproduce the experimental curves, as shown in Figure 6 by solid lines. Optimum rate constants were $k_{QB} = 5 \times 10^{10}$ [M^{-1} s^{-1}], $k_1 = 1.1 \times 10^{10}$ [M^{-1} s^{-1}], $k_2 = 3 \times 10^8$ [M^{-1} s^{-1}], and $\alpha \doteqdot 1$. The ratio of extinction coefficients is also obtained as $\epsilon(BP^{\bullet+}$ at 690 nm)/$\epsilon(NP^{\bullet+}$ at 860 nm) = 1.4 by the method described in the Appendix. Using the value reported in ref 18, the extinction coefficient of $NP^{\bullet+}$ at 860 nm is 8.2×10^3 M^{-1} cm^{-1}. All the rate constants obtained in this section are summarized in Table 1.

TABLE 1: Simulation Parameters Used for Figures 2, 4, and 6

species	parameters	values
CH_2Cl_2	r_0	33 (Å)
	Onsager length	65 (Å)
Cl^-	D	1×10^{-5} ($cm^2\ s^{-1}$)
biphenyl	k_{QA}	5×10^{10} ($M^{-1}\ s^{-1}$)
naphthacene	k_{QB}	5×10^{10} ($M^{-1}\ s^{-1}$)
	k_1	1.1×10^{10} ($M^{-1}\ s^{-1}$)
	k_2	3×10^8 ($M^{-1}\ s^{-1}$)
	α	~1
	ϵ(NP:860 nm)/ϵ(BP:690 nm)	1.4
	ϵ(NP:860 nm)	8.2×10^3 ($M^{-1}\ cm^{-1}$)
rubrene	k_{QB}	2×10^{10} ($M^{-1}\ s^{-1}$)
	k_1	0.65×10^{10} ($M^{-1}\ s^{-1}$)
	k_2	1.1×10^8 ($M^{-1}\ s^{-1}$)
	α	~1
	ϵ(RB:920 nm)/ϵ(BP:690 nm)	1.5
	ϵ(RB:920 nm)	8.8×10^3 ($M^{-1}\ cm^{-1}$)

Analysis of Intersolute Hole Transfer from $BP^{•+}$ to RB. The 3D result of pulse radiolysis for the mixed solution of BP (10 mM) and RB (0.8 mM) in DCM is shown in Figure 1S. The magnitude of the transient absorption is smaller than those in Figure 3. This is due to both the difference in the pulse charge and the difference in the optical alignment for the absorption measurement. The analysis of this system was performed in the same manner as for the BP + NP system (not shown). Reaction 24 was also observed. Optimized parameters were $k_{QB} = 2 \times 10^{10}$ [$M^{-1}\ s^{-1}$], $k_1 = 0.65 \times 10^{10}$ [s^{-1}], $k_2 = 1.1 \times 10^8$ [$M^{-1}\ s^{-1}$], $\alpha \doteqdot 1$, and $\epsilon(BP^{•+}$ at 690 nm)/$\epsilon(NP^{•+}$ at 920 nm) = 1.5. The extinction coefficient of $RB^{•+}$ at 920 nm was 8.75×10^3 $M^{-1}cm^{-1}$ also from the value reported in ref 18.

Hole Transfer Reaction. The obtained rate constants and other parameters used in the simulation for NP and RB systems are summarized in Table 1. Reported values of oxidation potentials (E_{ox}) in CH_2Cl_2[12] and ionization potentials (IP) in the gas phase are given in Table 1S.[10,11] Because of the extremely high IP (8.2 eV) of BP, its E_{ox} cannot be obtained by the electrochemical method. Therefore, ΔIP's are shown in Table 1S instead of ΔG's.

In our experiment, k_1 is expressed using the rate constant of the diffusion-controlled reaction k_{diff} and that of pure hole transfer k_{HT}.

$$1/k_1 = 1/k_{diff} + 1/k_{HT} \tag{26}$$

ΔIP's of the present systems are in the range 2.2−2.4 eV and should be located in the inverted region of Marcus's theory.[4] However, our experimental results indicate that k_{HT} is as large as, or larger than k_1 = 0.65−1.2 × 10^{10} [$M^{-1}\ s^{-1}$], the magnitude of which seems to be of almost pure diffusion. Extremely large k_{HT} implies that the hole transfer progresses via the excited states of $NP^{•+}$ and $RB^{•+}$ which are located >1 eV above the ground state. In this case of $k_{HT} \gg k_1$and $k_{diff} \approx k_1$, the difference in k_1 between NP and RB may reflect the difference in the molecular size of these molecules because the electronic structures of $NP^{•+}$ and $RB^{•+}$ are almost identical, as previously stated by Shida.[23] Molecular size dependence is also observed for IP − E_{ox} values, which indicate that the solvation of $NP^{•+}$ is more tight than that of $RB^{•+}$.

Extra Oxidation (Ionization) Process of NP and RB. The newly found oxidation process (24) possesses a second-order rate constant of $k_2 = 3 \times 10^8$ [$M^{-1}\ s^{-1}$] for NP and $k_2 = 1.1 \times 10^8$ [$M^{-1}\ s^{-1}$] for RB. Their pseudo-first-order kinetics indicates the existence of oxidants of with concentrations far smaller than [NP] or [RB]. Moreover, the value of $\alpha \doteqdot 1$ indicates that the unknown counterpart is produced approximately one at each ionization event.

There should be several candidates for the oxidant promoting this side reaction. One is a group of peroxy radicals ($CH_2ClO_2^•$ and $CHCl_2O_2^•$)[28] formed in aerated CH_2Cl_2 solutions on irradiation with assumption that our method of degassing is not sufficient. However, it has been reported that the oxidation process of these radicals are normally slow (in the order of 10^5 $M^{-1}\ s^{-1}$) even for the solute with a low ionization potential such as ZnTPP, which is comparable with NP and RB.[28] Therefore, these peroxy radicals are not the oxidant in this side reaction.

Another candidate is a strong oxidant $Cl^•$ formed in reaction 8 and/or (8′) although its concentration should be remarkably small. However, Alfassi et al.[27] estimated the lifetime of $Cl^•$ in the neat irradiated DCM and concluded that all chlorine atoms react with DCM within <0.1 μs in the absence of other reactive solutes as

$$Cl^• + CH_2Cl_2 \rightarrow CHCl_2^• + HCl \tag{27}$$

On the other hand, Sumiyoshi et al.[32a] reported the formation of a charge transfer (CT) complex between a chlorine atom and a solute molecule such as DMSO (demethyl sulfoxide) in the irradiated solution of DCM. A number of complexes formed with aromatic hydrocarbons are also reported in photochemical studies.[32] This complex can survive longer than several hundred nanoseconds and can act as a storage of chlorine atoms. The resultant radical $CHCl_2^•$ in (27) can also react as an oxidant with a long lifetime. However, the concentration of each three candidates, $Cl^•$, $Cl^•$−solute CT complex, and $CHCl_2^•$ should be far smaller than that of the ionizing event. The only candidate that satisfies $\alpha \approx 1$ is the $CH_2Cl^•$ radical formed from reaction 6.

The reported value[18] of ϵ at 690 nm of $BP^{•+}$ is 5.8×10^3 $M^{-1}cm^{-1}$. The maximum value of [$BP^{•+}$] in 100 mM solution (2 cm cell path length) directly estimated from the time profiles in Figure 2 is 2.6×10^{-5} M. The order of this value (0.01−0.1 mM) should be close to that of [$CH_2Cl^•$], which is compatible with the pseudo-first-order kinetics. This radical can easily escape from the spur and react with any species in the bulk solution. Its degradation process has not been clarified but is believed to decrease by a radical−radical recombination, which is very slow for 0.01 mM. Therefore, almost all of these radicals survive within the present time duration and may react with NP and RB in bulk such that

$$NP + CH_2Cl^• \rightarrow NP^{•+} + CH_2Cl^- \tag{28}$$

or

$$NP + CH_2Cl^• \rightarrow NP^{•+} + CH_2 + Cl^- \tag{29}$$

Since these reactions are a kind of electron transfer with charge separation, solvation energy and Coulomb stabilization energy can be gained. Although this radical is frequently referred to as a nucleophilic reagent in organic chemistry, it has been regarded as a silent species in radiation chemistry probably because it lacks absorption bands suitable for the pulse-radiolysis observation.

Similar reduction of aromatic hydrocarbon by neutral radicals has been reported in pulse radiolysis experiments on irradiated solutions of alcohol containing SF_6 as an electron scavenger.[33] The rate of oxidation of anthracene observed in that study is

compatible with our present result. The authors also provided two possibilities: with and without elimination of halogen anion.

Moreover, process (29) is preferred since spin change may occur coincidentally with the electron transfer process. When the initial state of these reactions is a combination of one singlet molecule (NP) and one doublet molecule ($CH_2Cl^{\bullet}$), the triplet CH_2Cl^- ($^3CH_2Cl^-$) can be directly formed in the single step of (29). CH_2 is known to have a triplet ground state by which extra formation energy can be gained.

The reactions that occur after (28) or (29) are unclear but many possibilities must be considered because both (28) and (29) include several reactive products (e.g., CH_2) and newly formed geminate pairs. The average distance between the new geminate pair should depend on the excess energy of the electron transfer process. The fraction of the correlated geminate pair cannot be determined. The results of simulation in Figure 6 indicate that the degradation of $NP^{\bullet+}$ formed from (28) and (29) is sufficiently slow.

On the other hand, however, the right-hand side of (28) and (29) may conflict with our assignment to the electron transfer mechanism. The typical electron transfer length of 5−10 Å is far shorter than the mean value of the ion pair separation r_0 (33 Å) and the Onsager length (65 Å) that we used in the simulation. Geminate ion pairs newly formed from (28) or (29) may be separated in a very short distance, and the ion pair should recombine in a short moment. However, the $NP^{\bullet+}$ could survive sufficiently long, escaping from the counterpart Cl^-.

The detail of the recombination processes of $NP^{\bullet+}$ with Cl^- is still unknown, although we described all the geminate recombination processes with the same diffusion kinetics throughout the simulation. We performed the experiment with DCM/NP solution to generate $NP^{\bullet+}$, as shown in Figure 1; however, the positive hole scavenging by NP could not be completed due to the low solubility of NP in this solvent (a few millimolar). Under such a condition, both concentrations of $NP^{\bullet+}$ and Cl^- cannot obtained. Compared in the same concentration, the lifetime of $NP^{\bullet+}$ (free ion) is longer than that of $BP^{\bullet+}$ and this implies that some activation energy would exist in the reaction of $NP^{\bullet+}$ with Cl^-. The encounter process of these two ions is not the rate-determining process but the back electron transfer is. Moreover, there should be a possibility of long-range electron transfer for (28) and (29).

Ab Initio Molecular Orbital Calculation. To justify our prediction, we performed ab initio MO calculations to estimate the stabilization energy of reactions 28 and 29. As was pointed out previously, there may exist artificial difficulty in the evaluation of electron affinity using the MO theory.[34] There is also difficulty in introducing the effect of solvent molecules, and the MO calculation for ionic species in solution frequently provides inaccurate results. Moreover, energy evaluation for the species with an unpaired electron (radicals) is difficult because of the problem of electron correlation. Keeping these in mind, we concentrate on acquiring a qualitative explanation for the following two dissociative electron attachments (DEA),[27] which are examples of dissociative electron transfer (DET).[35]

$$CH_2Cl_2 + e^- \rightarrow CH_2Cl_2^{\bullet -} \rightarrow CH_2Cl^{\bullet} + Cl^- \qquad (30)$$

$$CH_2Cl^{\bullet} + e^- \rightarrow CH_2Cl^- \rightarrow CH_2{:} + Cl^- \qquad (31)$$

For (30), Luke et al.[36] have already presented an estimation of the electron affinity of the present systems using various calculations including both semiempirical and ab initio ones. They reported several findings on the selection of a computational method. (a) The structure, especially the planarity of the chloromethyl radical ($CH_2Cl^{\bullet}$) and the C−Cl bond length of $CH_2Cl_2^{\bullet -}$, depends strongly on the level of calculation. (b) The values of vertical electron affinity are greatly reduced when the electron correlation is included. They published their results of geometry optimization for $CH_2Cl_2^{\bullet -}$ with a C_{2v} symmetry but did not present a potential surface for nonsymmetrical dissociation in which one of the C−Cl bonds is longer than the other.[36] We performed UHF 6-31G* calculation with two C−Cl bonds fixed, the results are shown in Figure 2S. At some of the grid points, the SCF solution was not obtained and no data are indicated in the figure. A shallow potential minimum exists at a nonsymmetrical C_s structure for which the optimized parameters are shown in Table 2. This geometry seems to correspond to that of the complex ($CH_2Cl^{\bullet}...Cl^-$) rather than to that of a radical anion. This result is compatible with recent results of IR measurement and ab initio calculation obtained by Schweig et al.[37] They presented an optimized geometry without symmetrical restriction, which seems to indicate the same kind of complex ($CH_2Cl^{\bullet}...Cl^-$) as ours. The extremely long C−Cl bond (=3.2 Å) and its low bond order imply that this radical anion can be easily dissociated with the aid of solvation energy in liquids. The computational results strongly suggest that the DEA process (30) is favored in liquid solution.

Since we required more exact values of the formation energy for reaction 31 than those obtained from HF, we used the MP2 calculation. However, we simply concentrate on only the following computational sequence and obtain results comparable with those obtained by Luke et al.[34] (Step 1) The geometry was optimized with RHF (singlet) or UHF (doublet and triplet) calculation with the 6-31G* basis set. (Step 2) The electronic energy was obtained by MP2 calculation with the 6-31G* basis set for the optimized geometry of Step 1. Luke et al.[36] also referred to the possibility of misleading results when the electron affinity is estimated from the combination of RHF and UHF methods.

First we attempted to obtain an optimized geometry of the metastable species that formed after electron attachment (30) (the singlet and triplet ground states of CH_2Cl^-). A C_s symmetry was assumed for each intermediate; however, no stable structures were obtained for $^3CH_2Cl^-$. The optimized geometry of $^1CH_2Cl^-$ also seems to correspond to that of the ($CH_2...Cl^-$) complex rather than that of the carbanion with a loose C−Cl bond (∼2.1 Å). Therefore, we calculated the energy change along the dissociation path of CH_2Cl^- for both singlet and triplet states and show the results in Figure 7. Only the result of UHF calculation is given for the triplet state, but we confirmed that the difference between UHF and ROHF is less than 0.2 eV. Although an energy minimum exists for the singlet, the potential curve for the triplet is completely dissociative. The energy position of $CH_2Cl^{\bullet}$ is located above these two potential curves, as shown in Figure 7.

To examine the effects of the excess energy on the reaction path, we calculated the optimized geometry of $CH_2Cl^{\bullet}$ and CH_2 (both singlet and triplet) and formation energies using the same level of MO calculation of MP2 6-31G*/HF 6-31G*. For the geometry of $CH_2Cl_2^{\bullet -}$ and CH_2Cl^-, we adopted those of CH_2Cl_2 and $CH_2Cl^{\bullet}$, respectively, and the vertical electron affinity was determined for $(CH_2Cl_2^{\bullet -})_{vert}$, and each of $(^1CH_2Cl^-)_{vert}$ and $(^3CH_2Cl^-)_{vert}$ shown in Table 2.

At the equilibrium position of the chloromethyl radical where C−Cl = 1.718 Å, two vertical energies are also shown for $(^1CH_2Cl^-)_{vert}$, and $(^3CH_2Cl^-)_{vert}$ in Figure 7. Since three vertical species are at sufficiently high energy positions, DEA of this radical should be preferred rather than the formation of a metastable species of $^1CH_2Cl^-$.

TABLE 2: Computational Results of Ab Initio Molecular Orbital Calculation

	species	symmetry (RHF/UHF)	optimized geometry		total energy (hartree) 6-31G*/HF (optimization)	total energy (hartree) 6-31G*/MP2 (single point)
(1)	CH_2Cl_2	C_{2v} RHF	C−H	1.0740 Å	−957.985 177 1	−958.375 762 1
			C−Cl	1.7680 Å		
			H−C−H	111.120°		
			Cl−C−Cl	112.861°		
(2)	$CH_2Cl_2^{\bullet-}$ (vertical)	C_{2v} UHF	(same as for (1))		−957.866 528 2	−958.266 480 9
(3)[a]	$CH_2Cl_2^{\bullet-}$ (relaxed)	C_s UHF	C−Cl(1)	3.3999 Å	−958.000 753 0	−958.363 749 3
			C−Cl(2)	1.7482 Å		
			C−H	1.0680 Å		
			H−C−H	120.732°		
			H−C−Cl(1)	60.944°		
			H−C−Cl(2)	116.216°		
(4)	$CH_2Cl^{\bullet}$	C_s UHF	C−H	1.0702 Å	−498.461 075 7	−498.484 001 1
			C−Cl	1.7179 Å		
			H−C−H	122.350°		
			H−C−Cl	116.525°		
(5)	$^1CH_2Cl^-$ (vertical)	C_s RHF	(same as for (4))		−498.253 335 1	−498.521 782 9
(6)	$^3CH_2Cl^-$ (vertical)	C_s UHF	(same as for (4))		−498.102 442 0	−498.358 683 8
(7)[b]	$^1CH_2Cl^-$ (relaxed)	C_s RHF	C−H	1.0991 Å	−498.426 745 0	−498.675 041 4
			C−Cl	2.1581 Å		
			H−C−H	102.319°		
			H−C−Cl	93.027°		
(8)[c]	$^3CH_2Cl^-$ (relaxed)	C_s UHF	(not obtained)			
(9)[d]	$^1CH_2$	C_{2v} RHF	C−H	1.0971 Å	−38.872 370 4	−38.969 888 4
			H−C−H	103.046°		
(10)[d]	$^3CH_2$	C_{2v} UHF	C−H	1.0711 Å	−38.921 497 5	−39.003 309 6
			H−C−H	130.72 2°		
(11)[d]	Cl^-					−459.652 104

[a] This geometry corresponds to the ($CH_2Cl^{\bullet}$...Cl^-) complex rather than the dichloromethane radical anion ($CH_2Cl_2^{\bullet-}$). [d] This geometry corresponds to the (CH_2...Cl^-) complex rather than the chloromethyl anion (CH_2Cl^-). [c] No stationary point was obtained. [d] This value is used for the calculation of the formation energy.

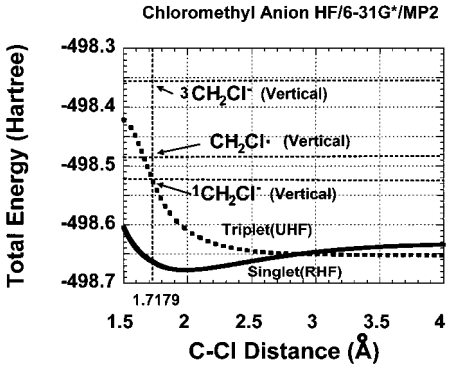

Figure 7. Potential curve for the dissociation of Cl^- from the singlet and the triplet state of CH_2Cl^- obtained by MP2 6-31G*//HF 6-31G*. The energy levels of $(^1CH_2Cl^-)_{vert}$ and $(^3CH_2Cl^-)_{vert}$ are indicated in the figure.

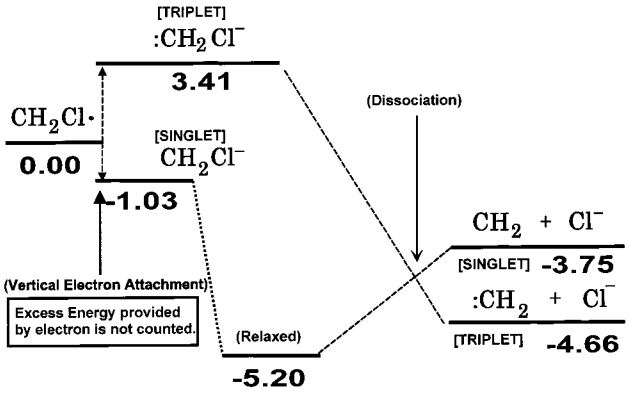

Figure 8. Born−Harber diagram concerning the dissociative electron attachment to $CH_2Cl^{\bullet}$ for both singlet and triplet states.

The Born−Haber diagram obtained is shown in Figure 8. This kind of approach has also been presented in ref 36 for the electron affinity of dichloromethane. Those results depend on the MO calculation, and the deviation width was found to be no less than 0.2 eV. Although they used experimental formation energies to reduce the effect of mismatch between UHF and RHF calculations, here we used only computational results to derive a self-consistent picture. The difficulty in estimating the electron affinity by MO calculation was previously discussed by Simons and Jordan.[34]

The formation energies of $(^1CH_2Cl^-)_{vert}$ and $(^3CH_2Cl^-)_{vert}$ through direct electron attachment are −1.03 and +3.41 eV, respectively, as shown in Figure 8. Since the energy level positions of $CH_2Cl^{\bullet}$, $(^1CH_2Cl^-)_{vert}$ and $(^3CH_2Cl^-)_{vert}$ are also indicated in Figure 7, the magnitude of geometrical relaxation can be found from the figure. The relaxed species of $^1CH_2Cl^-$ is located at −5.24 eV. The manifolds of the second dissociative electron attachment for the singlet (CH_2 + Cl^-) and triplet (CH_2: + Cl^-) states are located at 3.75 and 4.66 eV below the level of the chloromethyl radical, respectively.

Possibility of Dissociative Electron Transfer. The formation energy of dissociative electron attachment E_{at} is expressed as

$$E_{at} = \mathrm{IP(B)} + E_{EA} + E_{Solv} + E_C \qquad (32)$$

where IP(B), E_{EA}, E_{solv}, and E_C are the ionization energy of the second solute B, the formation energy of electron attachment

(including dissociative paths), the solvation energy, and the Coulombic energy, respectively. The ionization energy of the second solute for the present case (IP(B)) should be below 6 eV. The absolute value of E_{Solv} is smaller than 1 eV. E_c is about −4 eV at 3.5 Å or −1.3 eV at 10 Å. Therefore, if $E_{EA} \leftarrow 1.5$ eV, and even if we ignore the magnitude of computational error, this electron transfer reaction can proceed exothermically.

For this reaction process, both singlet and triplet states can be involved. The electron transfer with a charge separation is more favorable for the singlet path than for the triplet path. However, an activation energy exists for the dissociation path from the relaxed singlet species to a methylene and a chlorine anion. On the other hand, the triplet path is not favored for electron transfer but is advantageous to gain much energy upon the dissociation. If the entire process proceeds adiabatically, intersystem crossing should play an important role in this dissociation. However, the total process may be a concerted reaction and the nonequilibrium condition should be considered in each step. As long as the magnitude of the excess energy remains unknown, it is difficult to select one over the other two and both possibilities can be justified.

No slow formation of biphenyl radical cations was observed in our present experiment. The relatively high ionization energy of BP may regulate this by-passed oxidation. If so, the extremely low ionization energies of NP and RB are the most important factor in the efficiency of the total reaction.

Conclusion

In the course of the reinvestigation of the intersolute hole transfer reaction, we obtained evidence of a new oxidation process of aromatic hydrocarbons with low ionization energy, by the neutral radical $CH_2Cl^{\bullet}$, which is formed from the ejected electron. Ab initio molecular orbital calculation and analysis using the Smolchowski equation support this assignment. This is the first experimental result that indicates the possibility of the formation of two ion pairs in a single ionization event in the radiation chemistry of halogenated compounds.

Acknowledgment. The authors are grateful to Mr. Tohru Ueda and Mr. Toshiaki Kobayashi of the University of Tokyo for their help in pulse radiolysis experiments using LINAC at Tokai. Part of this study is supported by a Grant-in-Aid for Specially Promoted Research (No. 05237235) and a Grant-in-Aid for Encouragement of Young Scientists (No. 05740376, No. 06740466, and No. 07740481) from the Japanese Ministry of Education, Science, Sports, and Culture.

Appendix

Extraction of Each Component from Full 3-Dimensional Transient Absorption Data. To extract the kinetics of two components P and Q from three-dimensional transient absorption data, we performed the following numerical calculations.

First, from the measurements using a single solute, spectra of two components are obtained as $F_P(\lambda)$ and $F_Q(\lambda)$ in $\lambda_1 < \lambda < \lambda_2$. Normalized spectra are defined as

$$f_P(\lambda) = \frac{F_P(\lambda)}{\int_{\lambda_1}^{\lambda_2} F_P(\lambda)\, d\lambda} \qquad f_Q(\lambda) = \frac{F_Q(\lambda)}{\int_{\lambda_1}^{\lambda_2} F_Q(\lambda)\, d\lambda} \quad \text{(A1)}$$

The three-dimensional experimental data $D(t, \lambda)$ are also normalized as

$$d(t, \lambda) = D(t, \lambda)/N(t) \quad \text{(A2)}$$

where $N(t)$ is the time-dependent normalization factor:

$$N(t) = \int_{\lambda_1}^{\lambda_2} D(t, \lambda)\, d\lambda \quad \text{(A3)}$$

The normalized experimental data $d(t, \lambda)$ can be simulated using the autonormalized expression

$$s(t, \lambda) = x(t)\, f_P(\lambda) + (1 - x(t))\, f_Q(\lambda) \quad \text{(A4)}$$

where $0 \leq x(t) \leq 1$. For measurements at discrete points of wavelength λ_1, ..., λ_n, with equal separations, eqs A1−A3 are rewritten

$$f_P(\lambda) = \frac{F_P(\lambda)}{\sum_{i=1}^{n} F_P(\lambda_i)} \qquad f_Q(\lambda) = \frac{F_Q(\lambda)}{\sum_{i=1}^{n} F_Q(\lambda_i)} \quad \text{(A5)}$$

$$d(t, \lambda) = D(t, \lambda)/N(t) \quad \text{(A6)}$$

where

$$N(t) = \sum_{i=1}^{n} D(t, \lambda_i) \quad \text{(A7)}$$

If we assume autonormalization is also valid for the discrete data, $S(t, \lambda)$ in (A6) can be used as a good approximation for the experimental data. The most probable value of $x(t)$ is uniquely determined by a least-squares method to obtain

$$x(t) = \frac{\sum_{i=1}^{n} \{f_Q(\lambda_i) - d(t, \lambda_i)\}\{f_Q(\lambda_i) - f_P(\lambda_i)\}}{\sum_{i=1}^{n} \{f_Q(\lambda_i) - f_P(\lambda_i)\}^2} \quad \text{(A8)}$$

Finally, the simulation of the experimental data is obtained as

$$\begin{aligned} D(t, \lambda) &= c_P(t)\, f_P(\lambda) + c_Q(t)\, f_Q(\lambda) \\ &= N(t)\, x(t)\, f_P(\lambda) + N(t)(1 - x(t))\, f_Q(\lambda) \end{aligned} \quad \text{(A9)}$$

Therefore, the time profiles of each component can be expressed as

$$\begin{aligned} c_P(t) &= N(t)\, x(t) \\ c_Q(t) &= N(t)\, (1 - x(t)) \end{aligned} \quad \text{(A10)}$$

An example of simulation is shown in Figure 3S. The obtained kinetics $C_P(t)$ and $C_Q(t)$ for P = BP and Q = NP (the concentrations are [P] = 10 mM and [Q] = 0.8 mM in DCM) are indicated in Figure 3S. It should be noted that the values of $C_P(t)$ and $C_Q(t)$ tend to be erroneous when $x(t)$ is near zero or unity.

If the reaction is sequential such as P → Q or P + X → Q + Y, the decay of P coincides with the rise of Q, that is,

$$\frac{dc_P(t)}{d(t)} = -\kappa \frac{dc_Q(t)}{d(t)} \qquad \kappa > 0 \qquad \text{for all } t \quad \text{(A11)}$$

In this case, the ratio of the extinction coefficients can be simply expressed as

$$\frac{\epsilon_P(\lambda_P)}{\epsilon_Q(\lambda_Q)} = \kappa \frac{f_P(\lambda_P)}{f_Q(\lambda_Q)} \quad \text{(A12)}$$

Supporting Information Available: Figures absorption spectra and the potential surface and a table containing oxidation and ionization potentials. This material is available free of charge via the Internet at http://pubs.acs.org.

References and Notes

(1) Tabata, Y., Ed. *Pulse Radiolysis*; CRC Press: Boca Raton, FL, 1991.

(2) (a) Dorfman, L. M. *Acc. Chem. Res.* **1970**, *3*, 224. (b) Arai, S.; Grev, D. A.; Dorfman, L. M. *J. Chem. Phys.* **1967**, *46*, 2572. (c) Bockrath, B.; Dorfman, L. M. *J. Phys. Chem.* **1973**, *77*, 2618.

(3) (a) Shank, N.; Dorfman, L. M. *J. Chem. Phys.* **1970**, *52*, 4441. (b) Arai, S.; Ueda, H.; Firestone, R. F.; Dorfman, L. M. *J. Chem. Phys.* **1969**, *50*, 1072.

(4) (a) Marcus, R. A. *J. Chem. Phys*. **1956**, *24*, 966. (b) Marcus, R. A.; Sutin, N. *Biochim. Biophys. Acta* **1985**, *811*, 265 and references therein.

(5) (a) Miller, J. R. *Science* 1975, 221. (b) Beitz, J. M.; Miller J. R. *J. Chem. Phys.* **1979**, *71*, 4579. (c) Huddleston, R. K.; Miller, J. R. *J. Phys. Chem.* **1982**, *86*, 200. (d) Huddleston, R. K.; Miller, J. R. *J. Phys. Chem.* **1982**, *86*, 1347. (e) Huddleston, R. K.; Miller, J. R. *J. Chem. Phys.* **1983**, *79*, 5337. (f) Huddleston, R. K.; Miller, J. R. *J. Phys. Chem.* **1983**, *87*, 4867. (g) Miller, J. R.; Beittz, J. M.; Huddleston, R. K. *J. Am. Chem. Soc.* **1984**, *106*, 5057.

(6) (a) Closs, G. L.; Miller, J. R. *Science* **1988**, *240*, 440. (b) Calcaterra, L. T.; Miller, J. R.; Closs, G. L. *J. Am. Chem. Soc.* **1983**, *105*, 670. (c) Miller, J. R.; Calcaterra, L. T.; Closs, G. L. *J. Am. Chem. Soc.* **1984**, *106*, 3047. (d) Closs, G. L.; Calcaterra, L. T.; Green, N. J.; Remfield, K. W.; Miller, J. R. *J. Phys. Chem.* **1986**, *90*, 3673. (e) Johnson, M. D.; Miller, J. R.; Green, N. S.; Closs, G. L. *J. Phys. Chem.* **1989**, *93*, 1173.

(7) (a) Kira, A. *J. Phys. Chem.* **1981**, *85*, 3047. (b) Kira, A.; Nosaka, Y.; Imamura, M.; Ishikawa, T. *J. Phys. Chem.* **1982**, *86*, 1866. (c) Kira, A.; Imamura, M. *J. Phys. Chem.* **1984**, *88*, 1865.

(8) (a) Naleway, C. A.; Curtiss, L. A.; Miller, J. R. *J. Phys. Chem.* **1991**, *95*, 8434. (b) Curtiss, L. A.; Naleway, C. A.; Miller, J. R. *Chem. Phys.* **1993**, *176*, 387. (c) Curtiss, L. A.; Naleway, C. A.; Miller, J. R. *J. Phys. Chem.* **1995**, *99*, 1182.

(9) Reichardt, C. *Solvents and Solvent Effects in Organic Chemistry*, 2nd Completely Revised and Enlarged Edition; VCH: New York, 1990.

(10) Seki, K. *Mol. Cryst. Liq. Cryst.* **1989**, *171*, 255.

(11) (a) Kebarle, P.; Chowdhury, S. *Chem. Rev.* **1987**, *87*, 513. (b) Chen, E. C. M.; Wentworth, W. E. *Mol. Cryst. Liq. Cryst.* **1989**, *171*, 271.

(12) Bard, A. J.; Lund, H. *Encyclopedia of Electrochemistry of the Elements: Organic Section Vol XI* ; M. Dekker, New York, 1978.

(13) Fox, M. A. *Chem. Rev.* **1992**, *92*, 365 and all the references therein. See also all the articles in the same issue.

(14) Tabata, Y., Ito, Y., Tagawa, S., Eds. *Handbook of Radiation Chemistry*; CRC Press: Boca Raton, FL, 1981.

(15) (a) Rzad, S. J., *J. Phys. Chem.* **1972**, *76*, 3722. (b) de Haas, M. P.; Warman, J. M.; Infelta, P. P.; Hummel, A. *Chem. Phys. Lett*. **1974**, *31*, 382, **1976**, *43*, 321; *Can. J. Chem.* **1977**, *55*, 2249. (c) van den Ende, C. A. M.; Nyikos, L.; Warman, J. M.; Hummel, A. *Radiat. Phys. Chem.* **1980**, *15*, 273. (d) Sauer, M. C.; Jonah. C. D. *J. Phys. Chem.* **1980**, *84*, 2539.

(16) (a) Tagawa, S.; Washio, M.; Tabata, Y.; Kobayashi, H. *Radiat. Phys. Chem.* **1982**, *19*, 277. (b) Tagawa, S.; Washio, M.; Kobayashi, H.; Katsumura, Y.; Tabata, Y. *Radiat. Phys. Chem.* **1983**, *21*, 45. (c) Yoshida, Y.; Tagawa, S.; Tabata, Y. *Radiat. Phys. Chem.* **1984**, *23*, 279. (d) Yoshida, Y.; Tagawa, S.; Tabata, Y. *Radiat. Phys. Chem.* **1986**, *28*, 201. (e) Yoshida, Y.; Tagawa, S.; Kobayashi, H.; Tabata, Y. *Radiat. Phys. Chem.* **1987**, *30*, 83. (f) Yoshida, Y.; Tagawa, S.; Washio, M.; Kobayashi, H.; Tabata, Y. *Radiat. Phys. Chem.* **1989**, *34*, 493.

(17) (a) Smoluchowski, M. V. *Z. Phys. Chem. (Leipzig)* **1917**, *92*, 129. (b) Hummel, A. In *Kinetics of Nonhomogeneous Processes*; Freeman, G. R., Ed.; Wiley-Interscience: New York, 1987. **(**c) Keizer, J. *Chem. Rev.* **1987**, *87*, 187.

(18) (a) Hummel, A.; Luthjens, L. H. *J. Chem. Phys.* **1973**, *59*, 654. (b) Sehested, K.; Hart, E. J. *J. Phys. Chem.* **1975**, *79*, 1639. (c) Zador, E.; Warman, J. M.; Hummel, A. *J. Chem. Phys.* **1975**, *62*, 3897.

(19) (a) Shida, T.; Hamill, W. H. *J. Chem. Phys.* **1966**, *44*, 4372. (b) Thomas, J. K.; Johnson, K.; Klippert, T.; Lowers, R. *J. Chem. Phys.* **1968**, *48*, 1608. (c) Ueda, H. *Bull. Chem. Soc. Jpn.* **1968**, *41*, 2578. (d) Hamill, W. H. In *Radical Ions*; Kaiser, E. T., Kevan, L., Eds.; Wiley: New York, 1968; Chapter 9.

(20) Kobayashi, H.; Ueda, T.; Kobayashi, T.; Tagawa, S.; Tabata, Y. *Nucl. Instrum. Methods* **1981**, *179*, 223.

(21) Schmidt, H. W.; Baldridge, K. K.; Boatz, J. A.; Elbert, S. T.; Gordon, M. S.; Koseki, S.; Matsunaga, N.; Nguyen, K. A.; Su, S. J.; Windus, T. L.; Dupuis, M.; Montgomery, J. A. *J. Comput. Chem.* **1993**, *14*, 1347.

(22) The band due to solvent holes in halogenated compounds has not been established for liquid solution but has repeatedly been reported in matrix studies.

(23) Shida, T. *Electronic Absorption Spectra of Radical Ions*; Elsevier: Amsterdam, 1988.

(24) (a) Shpol'skii, E. V.; Il'ina, A. A.; Klimova, L. A. *Dokl. Akad. Nauk SSSR* **1952**, *87*, 935. (b) Orrit, M.; Bernard, J.; Personov, R. I. *J. Phys. Chem.* **1993**, *97*, 10256.

(25) Shida, T. Private communication.

(26) Tachiya, M. *Radiat. Phys. Chem.* **1987**, *30*, 75.

(27) Alfassi, Z. B.; Mosseri, S.; Neta, P. *J. Phys. Chem.* **1989**, *93*, 1380.

(28) (a) Grimshaw, J.; Langan, J. R.; Salmon, G. A. *J. Chem. Soc., Chem. Commun.* **1988**, 1115. (b) Bonazolla, L.; Michaut, J. P.; Roncin, R. *Chem. Phys. Lett.* **1988**, *153*, 52. (c) Chu, S. C.; Burrow, P. D. *Chem. Phys. Lett.* **1990**, *172*, 17. (d) Burrow, P. D.; Modelli, A.; Chiu, N. S.; Jordan, K. D. *J. Chem. Phys.* **1982**, *77*, 2699.

(29) (a) Hong, K. H.; Noolandi, J. *J. Chem. Phys.* **1978**, *68*, 5163−5172. (b) Noolandi, J. In *Kinetics of Nonhomogeneous Processes*; Freeman G. R., Ed.; John Wiley & Sons: New York, 1987; Chapter 9.

(30) (a) Washio, M.; Tagawa, S.; Tabata, Y. *Radiat. Phys. Chem.* **1983**, *21*, 239. (b) Washio, M.; Yoshida, Y.; Hayashi, N.; Kobayashi, H.; Tagawa, S.; Tabata, Y. *Radiat. Phys. Chem.* **1989**, *34*, 115. (c) Washio, M.; Tagawa, S.; Furuya, K.; Hayashi, N.; Tabata, Y. *Radiat. Phys. Chem.* **1989**, *34*, 533.

(31) For systems without the present assumption of unchanged geminate process, general formulations that can be used instead of (19)−(22) with slight modification have been presented by Tachiya.[26]

(32) (a) Sumiyoshi, T.; Katayama, M. *Chem. Lett.* **1987**, 1125. (b) Raner, K. D.; Lusztyk, J.; Ingold, K. U. *J. Phys. Chem.* **1989**, *93*, 564.

(33) Liu, A.-D.; Sauer, M. C.; Jonah, C. D. ; Trifunac, A. D. *J. Phys. Chem.* **1992**, *96*, 9293.

(34) Simons, J.; Jordan, K. D. *Chem. Rev.* **1987**, *87*, 535.

(35) (a) Chanon, M.; Tobe, M. L. *Angew. Chem. Int. Ed. Engl.* **1982**, *21*, 1. (b) Savêant, J.-M. *J. Am. Chem. Soc.* **1987**, *109*, 6788. (c) Andrieux, C. P.; Gallardo, I.; Savêant, J.-M.; Su. K.-B. *J. Am. Chem. Soc.* **1986**, *108*, 638. (d) Lund, T.; Lund, H. *Acta Chem. Scand. Ser. B* **1986**, *40*, 470; **1987**, *41*, 93.

(36) (a) Luke, B. T.; Loew, G. H.; McLean, A. D. *J. Am. Chem. Soc.* **1987**, *109*, 1307. (b) Luke, B. T.; Loew, G. H.; McLean, A. D. *J. Am. Chem. Soc.* **1988**, *110*, 3396.

(37) Richter, A.; Meyer, H.; Kausche, T.; Müller, T.; Sporleder, W.; Schweig, A. *Chem. Phys.* **1997**, *214*, 321.